arXiv:astro-ph/9811223v1 13 Nov 1998

Transmission and amplification of disturbances by massive halos

Chigurupati Murali
Canadian Institute for Theoretical Astrophysics, McLennan Labs, University of Toronto,
60 St. George St., Toronto M5S 3H8, Canada

ABSTRACT

We study how massive halos respond to perturbations. Through numerical solution of the coupled linearized Boltzmann-Poisson equations, we find that halos can transmit and amplify disturbances over large distances within galaxies. In particular, as Weinberg has noted, the halo provides an excellent medium for transmitting disturbances from the outer regions of galaxies to the inner regions. The dipolar response typically dominates and, in some cases, is very weakly damped. The monopole and quadrupole response can also make significant contributions. Overall, the results support the notion that disk structure can be excited by transmission of noise from the distant halo. The strong dipolar response suggests that halos play a role in producing lopsided disks. These results also suggest that, during formation from initial collapse, halos do not settle rapidly into static equilbrium; instead, they may continue to ring and interact with other embryonic components of proto-galaxies.

Subject headings: stellar dynamics – galaxies: individual (Milky Way) – galaxies: haloes – galaxies: kinematics and dynamics

1. Introduction

Galaxies typically inhabit noisy neighborhoods. Noise– or irregularites in the gravitational field– usually appears in the form of large satellites in the outskirts of galaxies (e.g. Zaritsky & White 1994). It is also expected in the form of continuing infall and inhomogeneity in the dark matter distribution. Yet most of this noise appears to lie at rather large distances. We might suppose, therefore, that it does not disturb the tranquility of the inner regions of galaxies, particularly galactic disks.

However, massive halos dominate most galaxies. They extend to large distances and, in some sense, provide a medium which potentially fosters communication between spatially separated regions, as Lynden-Bell (1985) first pointed out. Recent work by Weinberg (1995,1998) elucidates the dynamical behavior of this connective medium: the halo can respond to forcing by a satellite such as the LMC and efficiently transmit disturbances into the inner regions of galaxies. Consequently the apparent spatial isolation of inner regions is balanced by the halo's ability to transmit disturbances: the centers of galaxies seem to hear the noise, loud and clear.

Given the variety and ubiquity of disk structure, this might not come as a surprise. Galactic disks prominently display warps, lopsidedness, bars, spiral arms and other asymmetries. Theoretical work on disk structure shows that individual features are short-lived and must be continuously re-excited. Neverthess, it has been difficult to pinpoint the culprit since many candidate disturbers such as the LMC lie too far from the disk to excite structure through direct tidal forcing. Halo transmission and amplification seems to provide at least one necessary mechanism for continuously exciting disk structure (see Nelson & Tremaine 1995 for a comprehensive review of disk dynamics).

Unfortunately, it is difficult to study the response of halos to moderate amplitude perturbations. Ideally we could simply perform simulations. However, current N-body techniques suffer from resolution limitations due to particle number, drift in orbit integration and, in the case of expansion codes, inability to conserve momentum. These problems suppress linear collective effects which we expect to dominate the response in this regime.

An alternative approach, known as the 'matrix method', was originally developed to calculate dispersion relations of disk systems by Kalnajs (1977) and has been adapted by Weinberg (1989) to study spherical systems. The original implementation is best suited for stability analysis and determining the growth rates of unstable modes (e.g. Weinberg 1991; Saha 1992) because the dispersion relation is defined in the upper-half of the complex frequency plane. Recently, Weinberg (1994) modified the method to identify modes in stable systems using elegant numerical techniques to continue the dispersion relation into the lower half-plane.

In the present work, we further modify the matrix method in order to calculate the evolution of a perturbed system in time. In essence, we solve the coupled linearized Boltzmann-Poisson equations as an initial value problem to determine the linear response of the model system. Our approach is well suited to the study of stable galaxy response because the time-dependence and relative amplitudes of excited modes are uniquely determined for arbitrary external perturbations. Weinberg (1989,1995,1998) has taken a similar approach in calculating the response in the asymptotic limit of a periodic perturbation.

Herein we present the results of calculations using this method. Our results support the findings of Weinberg (1994,1995,1998) and demonstrate that halos can amplify perturbations and absorb energy into weakly damped oscillatory modes. Perhaps as importantly, the results demonstrate the need for high precision numerical calculations to study the subtle effects which determine the structure and evolution of galaxies. The outline is as folllows. We first derive the modification of the matrix method in §2. We then discuss the numerical implementation of the method and the battery of tests used to verify its accuracy in §3. The first section on results, §4, details the response of King models to point-like perturbations. Although not presented in a direct astrophysical context, these results demonstrate the variety of effects arising in the models and provide a convenient framework for categorizing the physical behavior. In the second section on results, §5, we present an example of a fly-by to illustrate how effects arise in an astrophysical

context. Several possibilities for further investigation are discussed in §6.

2. Formalism

2.1. Hamiltonian

We choose coordinates centered always on the unperturbed (monopole) potential. This introduces an *indirect term* into the Hamiltonian due to the acceleration of the reference frame. The resultant Hamiltonian then only describes the internal reaction of the unperturbed system to the perturbation. For tidal encounters, the indirect potential directly cancels the $\ell = 1$ component of the perturber's gravitational potential. However, for interpenetrating encounters, the term appears explicitly.

The full Hamiltonian is

$$H = \tfrac{1}{2}|\mathbf{v}|^2 + \Phi_0(|\mathbf{r}|) + \Phi^s(\mathbf{r},t) + \Phi^e(\mathbf{r},t) + \frac{d\mathbf{V}_c}{dt}\cdot\mathbf{r} \equiv H_0 + \Delta H. \tag{1}$$

The indirect term is given by the linear potential $d\mathbf{V}_c/dt\cdot\mathbf{r}$, where $d\mathbf{V}_c/dt$ is the mean acceleration of the unperturbed system. Defining the total potential perturbation $\Phi_1 = \Phi^s + \Phi^e$ as the respective sum of the response and direct external potentials, we can write

$$\frac{d\mathbf{V}_c}{dt} = -\frac{1}{M_c}\int d\mathbf{r}\rho_0\frac{\partial\Phi_1}{\partial\mathbf{r}} = \frac{1}{M_c}\int d\mathbf{r}\rho_1\frac{\partial\Phi_0}{\partial\mathbf{r}}, \tag{2}$$

where $\rho_1 = \rho^s + \rho^e$ is the respective sum of response and external source densities. The indirect term introduces a small modification of the matrix equation for the $\ell = 1$ component of the response. In these coordinates, the response contains no barycentric shift.

2.2. Linear theory and matrix method

The matrix method for determining the stability of stellar systems was originally developed by Kalnajs (1977). Our derivation is related to Weinberg's (1989) adaptation of the matrix method to spherical systems.

We consider the effect of weak perturbations on an equilibrium stellar system with distribution function $F(\mathbf{I})$ (hereafter DF), where the vector $\mathbf{I}$ denotes the actions associated with unperturbed orbits in the potential. Jeans' theorem states that the equilibrium DF does not depend on the angle variables $\mathbf{w}$ (Binney & Tremaine 1987). The evolution of the perturbed DF $f(\mathbf{I},\mathbf{w})$ is described by the linearized Boltzmann equation

$$\frac{\partial f}{\partial t} + \frac{\partial H_0}{\partial\mathbf{I}}\cdot\frac{\partial f}{\partial\mathbf{w}} - \frac{\partial F}{\partial\mathbf{I}}\cdot\frac{\partial\Delta H}{\partial\mathbf{w}} = 0, \tag{3}$$

where ΔH is the perturbing Hamiltonian defined above. The response potential Φ^s is related to f through Poisson's equation

$$\nabla^2\Phi^s = 4\pi G \int f d\mathbf{v} \equiv 4\pi G\rho^s. \tag{4}$$

In the non-self-gravitating approximation, one sets $\Phi_1 = \Phi^e$.

The perturbed quantities, f and ΔH, may be expanded in Fourier series in the action-angle variables of the unperturbed system (Goldstein 1980; Tremaine & Weinberg 1984). Following their convention, we define I_1 as the radial action, I_2 as the total angular momentum and I_3 as the z-component of the angular momentum. Motion in the unperturbed Hamiltonian $H_0(\mathbf{I}) = \frac{1}{2}|\mathbf{v}|^2 + \Phi_0(|\mathbf{r}|)$ is given by $\mathbf{I}$ = constant, $\mathbf{w} = \boldsymbol{\omega}t + \mathbf{w}_0$. In particular, the Fourier expansion of the perturbation becomes

$$\Delta H(\mathbf{r}, t) = \sum_{\mathbf{k}} \Delta H_{\mathbf{k}}(\mathbf{I}, t) \exp(i\mathbf{k}\cdot\mathbf{w}), \tag{5}$$

where

$$\Delta H_{\mathbf{k}}(\mathbf{I}, t) = \frac{1}{(2\pi)^3} \int d\mathbf{w} \Delta H(\mathbf{r}, t) \exp(-i\mathbf{k}\cdot\mathbf{w}). \tag{6}$$

Tremaine & Weinberg (1984) give expressions for the action-angle series of a multipole potential expansion: we introduce these formulae below.

Substituting into equation (3) yields the relation

$$\frac{\partial f_{\mathbf{k}}(\mathbf{I}, t)}{\partial t} + i\mathbf{k}\cdot\boldsymbol{\omega} f_{\mathbf{k}} = i\mathbf{k}\cdot\boldsymbol{\omega}\frac{dF}{dE}\Delta H_{\mathbf{k}}(\mathbf{I}, t), \tag{7}$$

since $\partial H_0/\partial\mathbf{I} = \boldsymbol{\omega}$ defines the vector of stellar orbital frequencies and $\partial F/\partial\mathbf{I} = \boldsymbol{\omega} dF/dE$ for an isotropic DF. We can construct the inhomogeneous solution to equation (7) from the homogeneous solution (right-hand side zero); therefore

$$f_{\mathbf{k}}(\mathbf{I}, t) = i\mathbf{k}\cdot\boldsymbol{\omega}\frac{dF}{dE}\int_{-\infty}^{t} dt' \exp[i\mathbf{k}\cdot\boldsymbol{\omega}(t'-t)]\Delta H_{\mathbf{k}}(\mathbf{I}, t'). \tag{8}$$

Summing over $\mathbf{k}$ and integrating over velocities yields a formal expression for the perturbed density:

$$\rho^s = \int d\mathbf{v} \sum_{\mathbf{k}} \exp(i\mathbf{k}\cdot\mathbf{w})(i\mathbf{k}\cdot\boldsymbol{\omega})\frac{dF}{dE}\int_{-\infty}^{t} dt' \exp[i\mathbf{k}\cdot\boldsymbol{\omega}(t'-t)]\Delta H_{\mathbf{k}}(\mathbf{I}, t'). \tag{9}$$

To determine the response density and potential, we first introduce biorthonormal expansions (e.g. Kalnajs 1977; Weinberg 1989) for the density,

$$\rho^s = \sum_{\ell m j} a_j^{\ell m}(t) d_j^{\ell m}(r) Y_{\ell m}(\boldsymbol{\Omega}), \tag{10}$$

and potential,

$$\Phi^s = \sum_{\ell m j} a_j^{\ell m}(t) u_j^{\ell m}(r) Y_{\ell m}(\boldsymbol{\Omega}). \tag{11}$$

The perturbing potential Φ^e has an analogous expansion in terms of coefficients denoted $b_j^{\ell m}(t)$. The condition of biorthonormality relates the basis functions through Poisson's equation

$$\nabla^2 u_i^{\ell m} = 4\pi G d_i^{\ell m}, \tag{12}$$

and imposes orthogonality,

$$-\frac{1}{4\pi G}\int dr r^2 u_j^{*\ell m} d_i^{\ell m} = \delta_{ij}. \tag{13}$$

To substitute into equation (9), we first rewrite these expansions in action-angle variables using expressions from Tremaine & Weinberg (1984). The coefficient

$$\Delta H_{\mathbf{k}} = \sum_\ell [a_j^{\ell k_3}(t) + b_j^{\ell k_3}(t)]\left[W_{\mathbf{k}}^{\ell j}(\mathbf{I}) + \frac{4\pi}{3} p_j^{\ell m} X_{\mathbf{k}}(\mathbf{I})\delta_{\ell 1}\right] V_{\ell k_2 k_3}(\beta), \tag{14}$$

where $\cos\beta = I_3/I_2$ and $V_{\ell k_2 k_3}(\beta)$ is defined in terms of rotation matrices. The second term in brackets on the right-hand side arises from the indirect potential. The Fourier coefficients have the definitions

$$W_{\mathbf{k}}^{\ell j}(\mathbf{I}) = \frac{1}{2\pi}\int_{-\pi}^{\pi} dw_1 \exp(-ik_1 w_1) u_j^{\ell k_3} \exp[ik_2(\psi - w_2)], \tag{15}$$

and

$$X_{\mathbf{k}}(\mathbf{I}) = \frac{1}{2\pi}\int_{-\pi}^{\pi} dw_1 \exp(-ik_1 w_1) r \exp[ik_2(\psi - w_2)]. \tag{16}$$

The angle $\psi - w_2$ has the definition

$$\psi - w_2 = \int_{r_p(\mathbf{I})}^{r(\mathbf{I},w_1)} \frac{dr(\omega_2 - I_2/r^2)}{\sqrt{2[E - \Phi(r)] - I_2^2/r^2}}. \tag{17}$$

Lastly,

$$p_j^{1m} = \int dr r^2 d_j^{1m} \frac{\partial \Phi_0}{\partial r}. \tag{18}$$

Now substituting these expansions into equation (9), taking the inner product with respect to $u_i^{\ell m *} Y_{\ell m}^*(\mathbf{\Omega})$, where

$$u_i^{\ell m *} Y_{\ell m}^*(\mathbf{\Omega}) = \sum_{\mathbf{k}'} V_{\ell k_2 k_3}^*(\beta) W_{\mathbf{k}}^{\ell i *}(\mathbf{I}) \exp(-i\mathbf{k}'\cdot\mathbf{w}), \tag{19}$$

and noting that $d\mathbf{r}d\mathbf{v} = d\mathbf{I}d\mathbf{w}$, we obtain a set of coupled integral equations for the expansion coefficients:

$$\begin{aligned} a_i^{\ell m}(t) \;=\; & -\frac{1}{4\pi G}\int d\mathbf{I} d\mathbf{w} \frac{dF}{dE} \sum_{\ell m i \mathbf{k}\mathbf{k}'} (i\mathbf{k}\cdot\boldsymbol{\omega}) \int d\tau \exp[i\mathbf{k}\cdot\boldsymbol{\omega}(\tau - t)][a_j^{\ell m}(\tau) + b_j^{\ell m}(\tau)] \\ & V_{\ell k_2' k_3'}^*(\beta) V_{\ell k_2 k_3}(\beta) W_{\mathbf{k}'}^{\ell i *}(\mathbf{I})\left[W_{\mathbf{k}}^{\ell j}(\mathbf{I}) + \frac{4\pi}{3} p_j^{\ell m} X_{\mathbf{k}}(\mathbf{I})\delta_{\ell 1}\right] \exp[i(\mathbf{k} - \mathbf{k}')\cdot\mathbf{w}] \end{aligned} \tag{20}$$

Integrating over angles yields $(2\pi)^3\delta_{\mathbf{k}\mathbf{k}'}$. To integrate over β, we employ the orthogonality relation of rotation matrices (Edmonds 1960):

$$\int d\cos\beta V^*_{\ell' k_2 k_3}(\beta) V_{\ell k_2 k_3}(\beta) = \frac{2}{2\ell+1}|Y_{\ell k_2}(\tfrac{1}{2}\pi, 0)|^2 \delta_{\ell'\ell} \equiv C_{\ell k_2}\delta_{\ell'\ell}, \tag{21}$$

where

$$\begin{aligned} C_{\ell k_2} &= \frac{2^{2k_2-1}}{\pi^2}\frac{(\ell-k_2)!}{(\ell+k_2)!}\left[\frac{\Gamma[\frac{1}{2}(\ell+k_2+1)]}{\Gamma[\frac{1}{2}(\ell-k_2)+1]}\right]^2, \ell+k_2 \quad \text{even} \\ &= 0 \qquad\qquad\qquad\

yields an equation for the Green's function

$$\rho^s_{\mathbf{r}_p,t_p}(\mathbf{r},t) = G_\rho(\mathbf{r},\mathbf{r}_p;t-t_p), \tag{29}$$

where the notation $\rho_{\mathbf{r}_p,t_p}$ indicates that the response is due to a point source at a particular location.

The linear response operator has a definition similar to that of G_ρ (Nelson & Tremaine 1997):

$$\rho^s(\mathbf{r},t) = \int d\mathbf{r}'dt' R(\mathbf{r},\mathbf{r}';t-t')\Phi^e(\mathbf{r}',t'). \tag{30}$$

Comparing equations (27) and (30) shows that the Green's function and linear response operator have the following relation:

$$R(\mathbf{r},\mathbf{r}';t-t') = G_\rho(\mathbf{r},\mathbf{r}';t-t')(4\pi G)^{-1}\nabla^2_{\mathbf{r}'} \tag{31}$$

The method defined above provides a numerical definition of the Green's function or linear response operator for a system.

3. Numerical implementation and tests

We use standard numerical techniques to implement the method. There are three basic components: the action-angle expansions, the basis function expansions and the solution of the coupled integral equations. Angles and frequencies are computed from the orbit equations on a 120×20 grid in E and J, respectively, with $k_1 \leq 4$. Calculations with $k_1 \leq 8$ produced the same results: higher-order resonance influence damping at small spatial scales rather than the large scales of interest here. We use the Hernquist basis for the biorthogonal expansion and truncate the series after 30 radial terms. The coupled integral equations are solved iteratively to a tolerance of 10^{-6} using Simpson's rule on a 1024-point grid to evaluate the lag time quadrature in equation (24) for $\tau \geq t - 200$.

In practice, we first compute the angles, frequencies and Fourier coefficients of the basis functions for a particular model and ℓ and dump the results to a file using an unformatted output stream. Taking this data as input, we then compute the response kernel in equation (24) and again save the results using an unformatted output stream. Computing the kernel takes the most time– roughly 3 hours on a fully loaded SGI origin. However, given the kernel, we can calculate the response to any perturbation in short order.

We performed three tests of the implementation. The simplest was to reproduce the analytic adiabatic fluid response calculation for both the isothermal sphere (Murali & Tremaine 1997) and a $W_0 = 5$ King model. This provides a test of the spatial response which is independent of the temporal response. It ensures that the basis function expansion works properly and that a sufficient number of terms have been retained to correctly reproduce the potential and

density response. We then tested the accuracy of the spatial and temporal solution by Laplace transforming the response coefficients along a strip in the complex plane and plugging these values into the dispersion relation, equation (25)[1]. The transforms of the dominant coefficients typically satisfy the dispersion relation to within at least 10%.

Finally, as a straightforward but important check, we compare in Figure 1 the results of our linear calculation with an N-body simulation performed with the self-consistent-field code discussed most recently by Hernquist & Ostriker (1992). The code employs the identical multipole-biorthonormal decomposition of the potential used in the linear calculation developed above. Thus we may directly compare the time evolution of expansion coefficients computed using the two methods. We find good agreement for $\ell = 2$.

Given the results below, we are particularly interested in comparing the two calculations for $\ell = 1$. However, we were unable to reproduce the calculated response using an SCF simulation with 10^6 particles. As Weinberg (1994) notes, expansion codes do not conserve momentum, so they will be hard-pressed to reproduce an off-center response since the center wanders. In particular, to defeat wandering, the standard centering algorithm calls for resetting the coordinate center to the center-of-mass of the system at each potential recomputation. However, to recognize and reproduce a dipole response we should ideally remain in a reference frame which is attached to the center of the unperturbed potential (which is no longer at the center-of-mass because of the dipole response). Nevertheless, experiments without the centering algorithm also failed to reproduce the effect.

4. Response to point-like perturbations

In the spirit of calculating the Green's function, we subject the model systems to point-like perturbations:

$$\Phi^e(\mathbf{r}) = \delta(t)\Phi_p(|\mathbf{r} - \mathbf{r}_p|) \tag{32}$$

where $\Phi_p(\mathbf{r}_p)$ denotes the potential of a point-mass of mass m_p located at $\mathbf{r}_p$ (for definiteness, the angular coordinates $\theta_p = \phi_p = 0$). Point-like perturbations also approximate Poisson fluctuations in equilibrium systems.

We impose perturbations of harmonic order $\ell = 0, 1, 2$ and corresponding m values on a range of King models at radii enclosing different mass fractions of the unperturbed system. Table 1 outlines the computational grid. The notation r_x denotes the radius enclosing the fraction x of the total mass of the system. The quantity r_t denotes the tidal radius or radius enclosing 100% of the mass.

Units are defined such that the total mass $M = 1$, $G = 1$ and the total energy $E = -1/8$.

[1]Suggested by John Dubinski

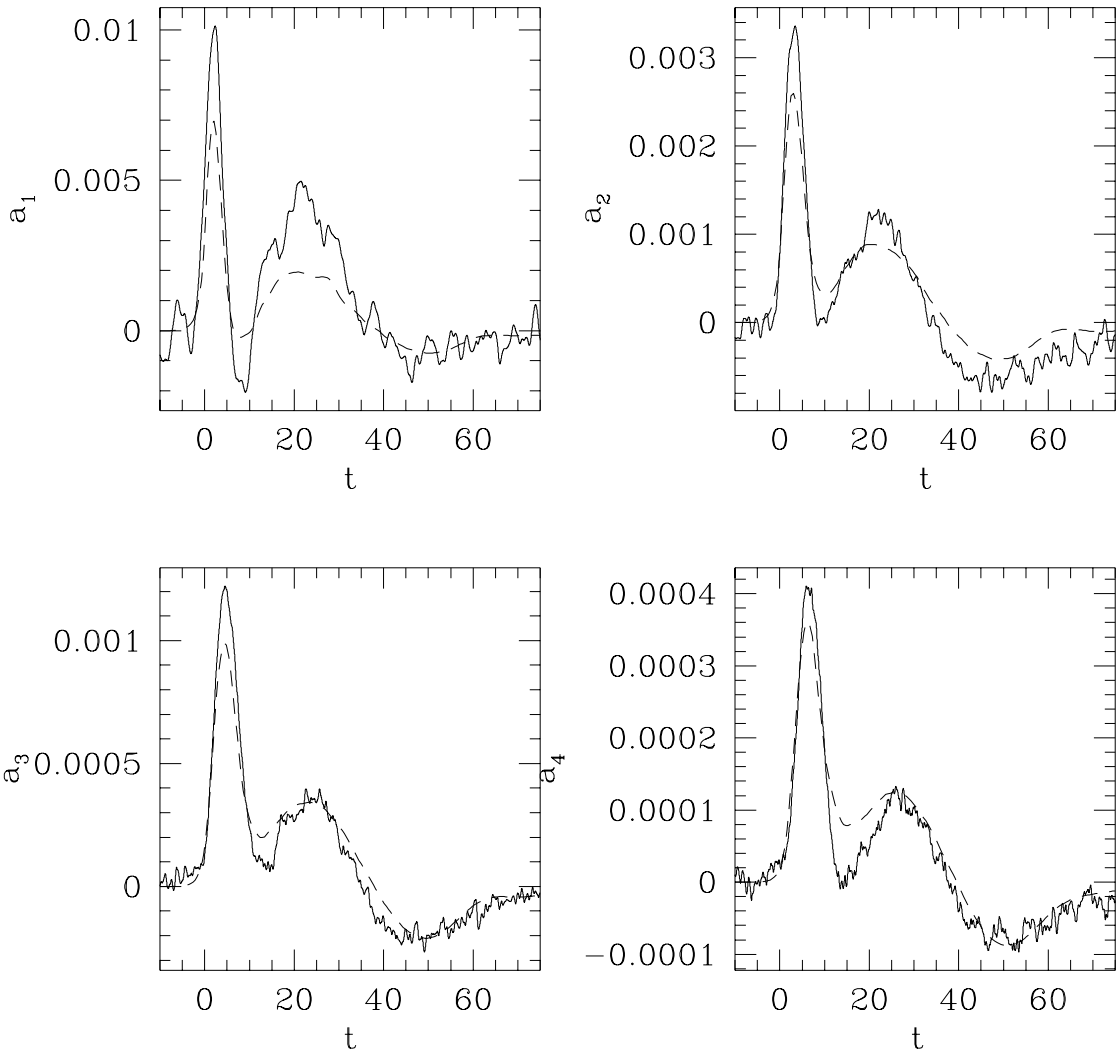

Fig. 1.— The self-gravitating response of a $W_0 = 5$ King model to an $\ell = 2$, $m = 0$ perturbation which is turned on and off exponentially. The four lowest order expansion coefficients are plotted in time for the linear calculation (dashed) and N-body simulation (solid) with 10^6 particles.

This implies that, at $r_{1/2}$, the period of a circular orbit, $P_{1/2} \sim 18$. Reaonable physical values can be obtained by rescaling the models to halos of mass $M = 10^{12} M_\odot$ and limiting radius $r_{max} = 200\,\mathrm{kpc}$.

We set the perturbation amplitude by adjusting m_p. Our choices are arbitrary and serve more to illustrate the physics of the response. For distant perturbations $M(r_p) > 0.75$, we typically choose $m_p = 0.1$ while for inner perturbations $M(r_p) < 0.75$, we typically choose $m_p = 0.01$. Since the calculation is linear, we may rescale the results for other choices of m_p.

4.1. Transmission and amplification of disturbances

We find that significant transmission and amplification of disturbances can occur in the model calculations. Since the response to each ℓ is independent, we consider each separately.

4.1.1. Monopole response

The monopole component of the perturbation acts like a spherical shell of mass m_p which exerts a force only on material at $r > r_p$, the shell radius. This generates a density enhancement at $r > r_p$ which propagates inward to smaller radii. Figure 2 shows this effect in a $W_0 = 3$ King model. We find that the amplitude of the propagating response can be significant well within the radius of the perturbation. Since the monopole component of the perturber's direct gravitational field exerts no force on material with $r < r_p$, the amplification is infinite.

Deeper within the $W_0 = 3$ system, smaller perturbations give rise to similar effects in the core. For perturbations at the 25% mass fraction, we find a roughly a 1% central response for $m_p = 0.01$. The amplitude of the peak central density response decreases with concentration due to the increasing depth of the central potential well.

Table 1: Characteristics of King models and computational grid

W_0	c	$r_{1/4}$	$r_{1/2}$	$r_{3/4}$	r_t
3	0.7	1.1	1.7	2.4	6.2
5	1.0	1.0	1.6	2.6	8.7
7	1.5	0.8	1.6	3.2	14

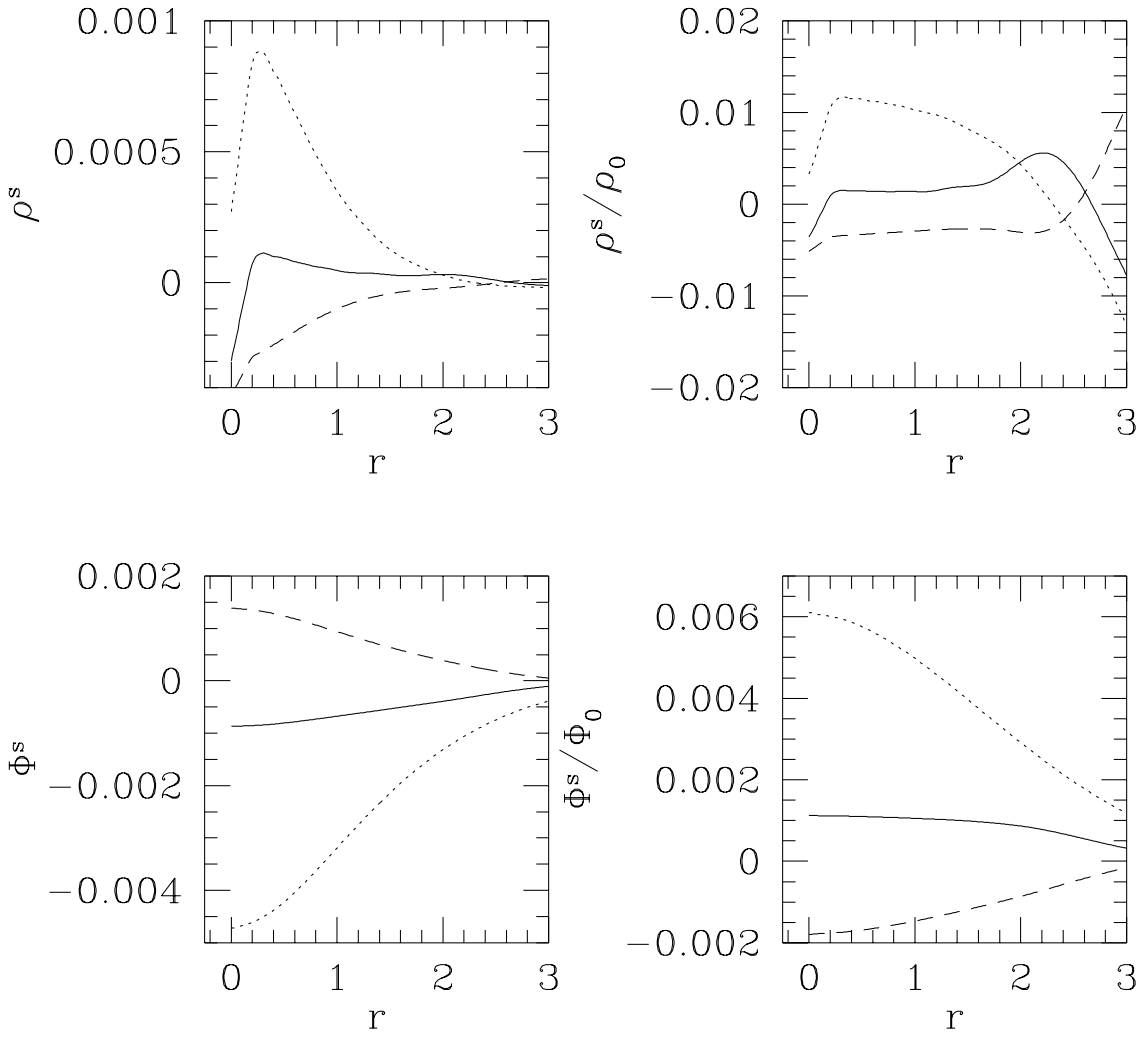

Fig. 2.— Transmission of spherical disturbance in $W_0 = 3$ King model initially excited at $r_p = 2.4$ (75% mass radius) for $m_p = 0.1$. Panels show density, potential and respective contrasts as a function of radius as indicated. In each panel, solid line shows inwardly growing response at $t = 1.1$ following perturbation. Dotted line shows peak central response at $t = 5.8$. Dashed line shows subsequent minimum at $t = 12.8$ as disturbance propagates outwards. The perturbation subsequently damps away. The peak central density response is roughly 1%.

4.1.2. Dipole response

The dipole component of the perturbation acts somewhat differently from the monopole in that it exerts a force at all radii. Some component of this force contributes to the mean motion of the system; recall that the indirect potential removes this component in the present calculation. Nevertheless, the residual (differential) acceleration excites a strong dipolar response in all the models studied here.

For each of the King models, Table 2 shows the basic response characteristics for perturbations at the 75% mass radius. The response travels deep into the system, producing peak density contrast at roughly $0.1r_p$ (radius denoted r_{peak} enclosing $M(r_{peak})$ of the total mass). In each case, the fractional density response is several %. The response improves with concentration. Also note that there may be a substantial delay between the application of the perturbation and the peak response in the system's core at t_{peak}.

Figure 3 provides a close look at a cross-section of the response in the $W_0 = 7$ system. The density at small radii responds strongly to the perturbation. To better understand this effect, we show the cross section of the mass perturbation $r^2\rho^s$ along $\mathbf{r}_p$ in Figure 4. The perturbation draws mass from all surrounding directions. However, mass drawn from inner regions produces a large change in the density because of the smaller volume.

To gauge the importance of self-gravity, it is useful to compute the amplification factor or Love number of the perturbation: $\chi \equiv (\Phi^s + \Phi^{e\prime})/\Phi^{e\prime}$, where $\Phi^{e\prime}$ includes the indirect term[2]. Figure 5 shows χ for the perturbation depicted in the previous figure. The $W_0 = 7$ system achieves dipole amplification factors of 10 or so which may persist for long durations in weakly damped modes. Such strong amplification will lead to non-linear effects that are not described by our present treatment. The amplification factors decrease with concentration: for $W_0 = 5$, $|\chi| \sim 4$; for $W_0 = 3$, $|\chi| \sim 2$.

Similar effects result from disturbances at smaller radius. These lead to stronger effects in the core. Table 3 shows the peak central response arising from a point perturbation at the radius enclosing 50% of the mass. Here disturbances are transmitted to small radius. Disturbances at

[2]There is apparently some ambiguity in defining χ for $\ell = 1$: we have chosen Φ^s as the total potential perturbation and $\Phi^{e\prime}$ as the external potential which produces Φ^s.

Table 2: Peak central density contrast for $M(r_p) = 0.75$ and $m_p = 0.1$

W_0	r_p	r_{peak}	$\lvert\rho^s/\rho_0\rvert$	$M(r_{peak})$	t_{peak}
3	2.4	0.2	0.03	0.01	5.8
5	2.6	0.3	0.04	0.02	5.8
7	3.2	0.3	0.05	0.03	8.1

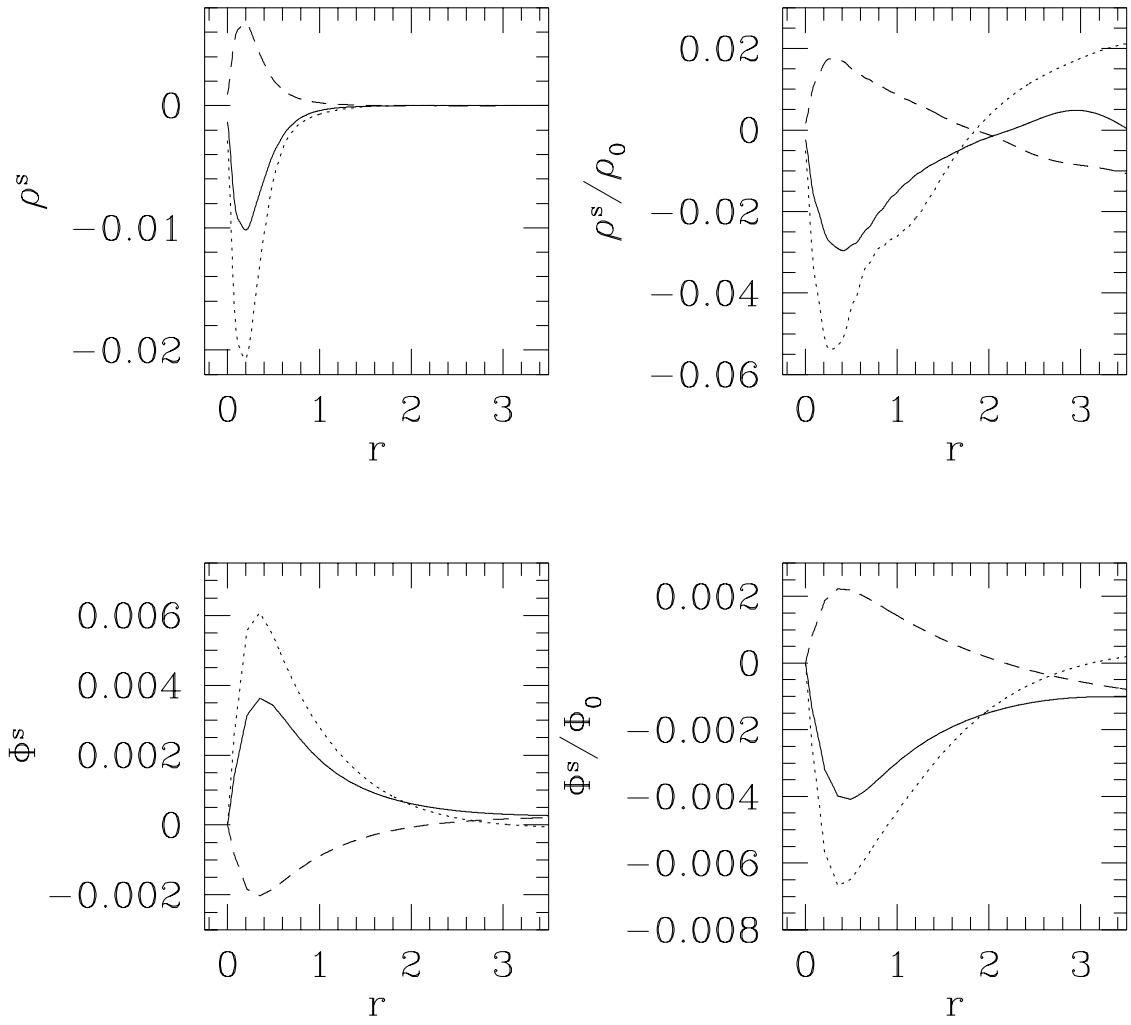

Fig. 3.— Transmission of dipole disturbance in $W_0 = 7$ King model initially excited at $r_p = 3.2$ (75% mass radius) for $m_p = 0.1$. Panels are as in previous figure with radial profile along $\mathbf{r}_p$. Solid line shows growing response at $t = 3.4$ following perturbation. Dotted line shows peak central response at $t = 8.1$. Dashed line shows large subsequent peak after next half-cycle of mode oscillation at $t = 38.6$, indicating the presence of weakly damped modes with very slow pattern speeds. The peak inner density response is roughly 5%, dropping to $\sim 2\%$ after the next half-cycle.

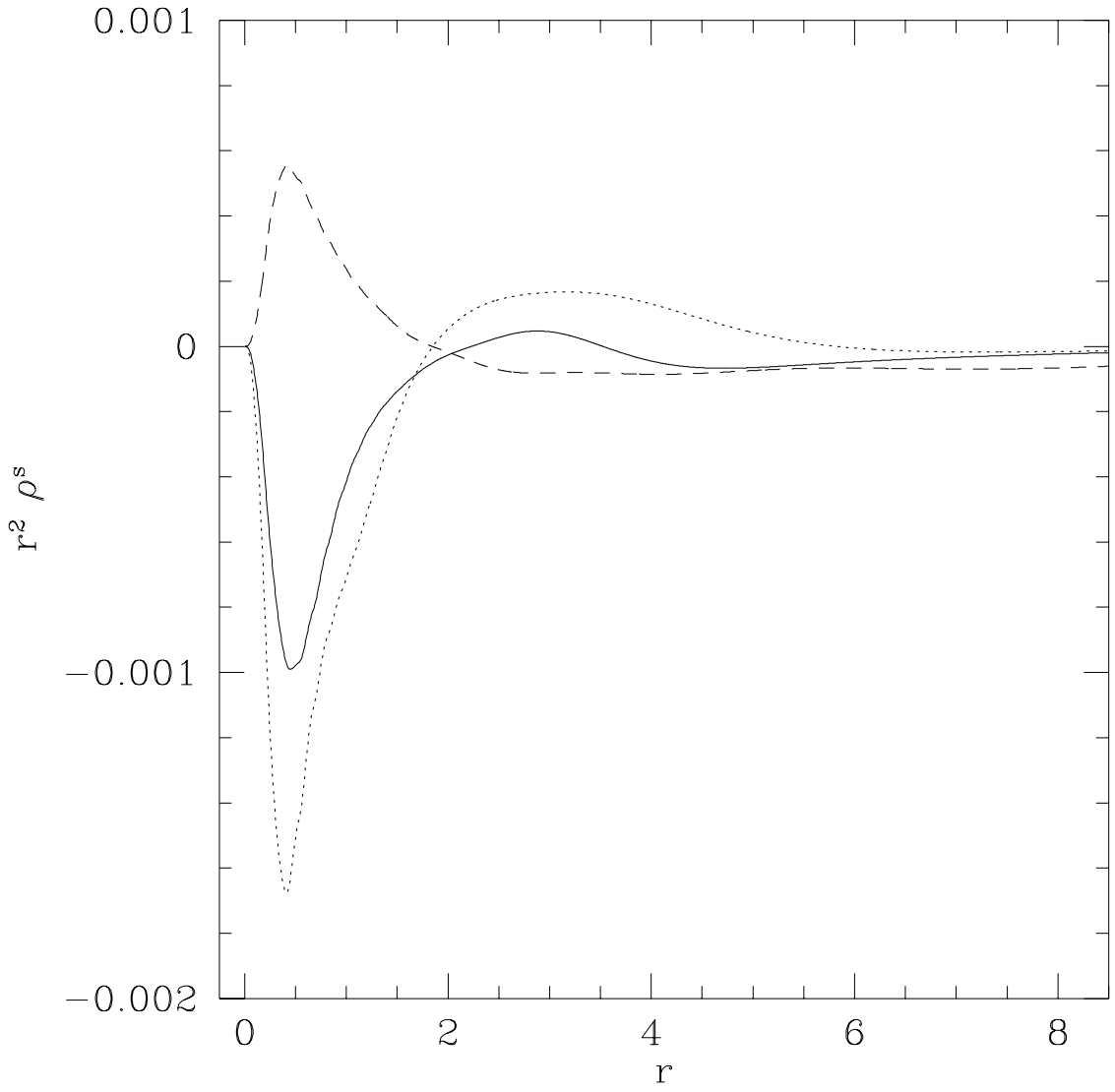

Fig. 4.— The change in mass along the $\mathbf{r}_p$ axis corresponding to the perturbation depicted in the previous figure. At $t = 3.4$, mass is attracted towards the perturber's original position ($r_p = 3.2$; solid). This draws material from surrounding regions, but affects the density small radius because of the smaller volume. At $t = 8.1$, the response peaks (dotted). Finally, after the next half-cycle ($t = 38.6$), the response peaks again (dashed).

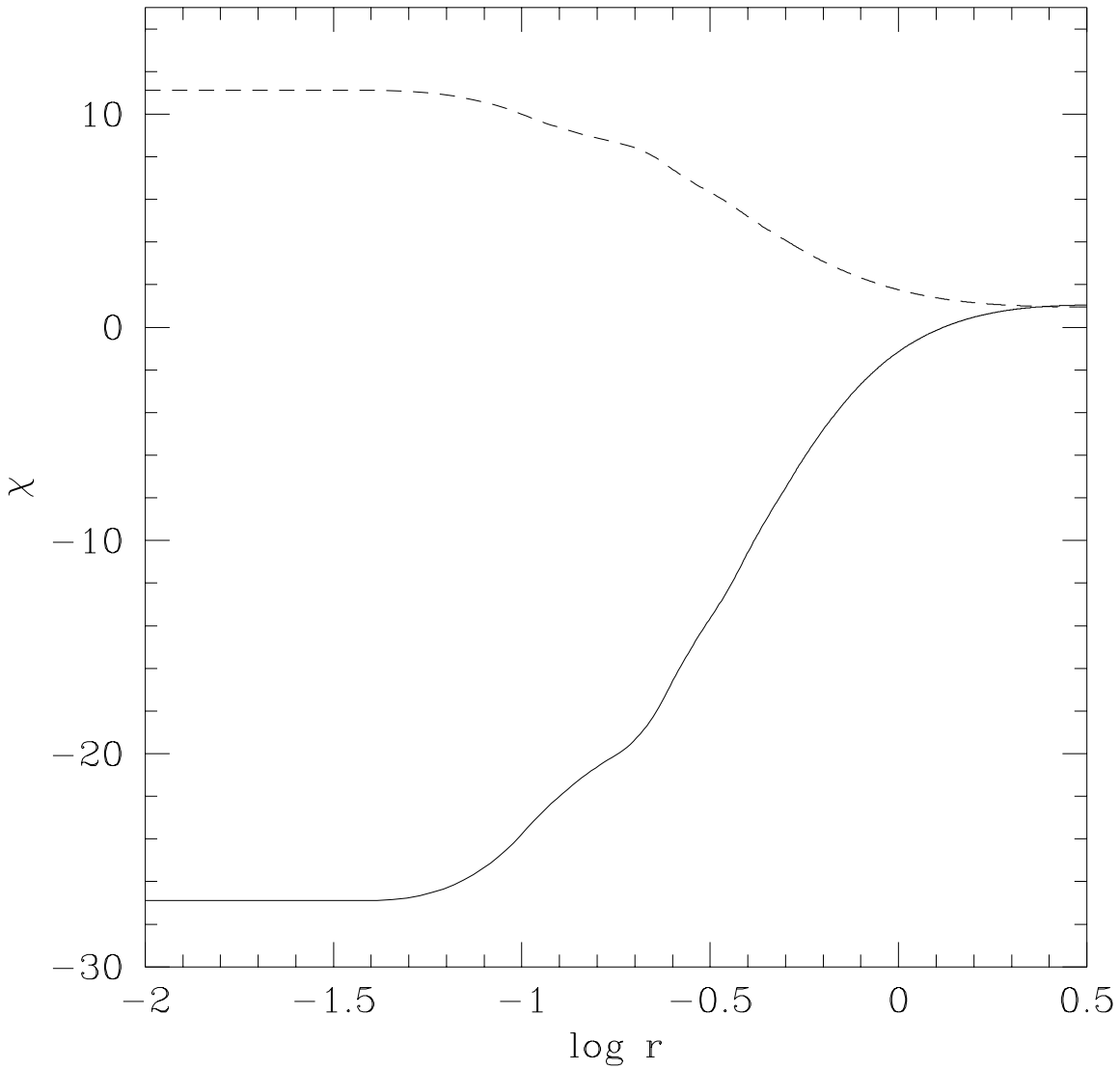

Fig. 5.— Potential amplification factor χ along $\mathbf{r}_p$ for disturbance shown in figure 4.1.2 ($\log r_p = 0.5$). Solid line shows amplification at peak response ($t = 8.1$). Dashed line shows amplification at peak after next half-cycle ($t = 38.6$). On the near side of the disturbance, de-amplification of the potential perturbation weakens the interior halo potential while, on the far side, de-amplification strengthens. The amplification magnitude is roughly 10 and can persist for long times after the disturbance disappears, due to the excitation of weakly damped modes.

even smaller radius can excite the dominant response directly.

4.1.3. Quadrupole response

In these experiments, quadrupole disturbances do not appear to propagate from large radius to small radius in the same manner as monopole and quadrupole disturbances. Figure 6 shows an example of the response to an $\ell = 2$, $m = 2$ perturbation in a $W_0 = 5$ King model. The main feature is the local density response which then decays away relatively rapidly. This tends to produce moderate amplifications of $\sim 30\%$ at radii roughly $0.3r_p$. Overall, the quadrupole response appears to be most important in the case of pure resonant forcing (Weinberg 1998).

5. A realistic example of dipole response

The above analysis details the physical behavior of the response. To provide a more realistic example focusing in the $\ell = 1$ response, we take a point-mass perturber with $m_p = 0.01$ on a hyperbolic trajectory through a $W_0 = 7$ halo. The perturber initially has velocity $v = 0.5$ at infinity: this is roughly the circular speed at the half-mass radius. Closest approach is at $r = 2.6$, the radius enclosing 68% of the total mass. The maximum velocity is roughly $v = 1.0$ so that the effect of dynamical friction will be small. Figure 7 shows the strong $\ell = 1$ response induced by the relatively small perturber.

The encounter excites a very weakly damped mode. Figure 8 shows the time-dependence of the induced potential energy perturbation which provides a good signature of mode oscillation. For comparison, Weinberg (1994) found an e-folding $2\pi/\,Im(\omega) = 250$ and an oscillation period $2\pi/\,Re(\omega) = 98$ in these units for $W_0 = 7$. The response depicted here shows an oscillation period $P \approx 100$ in good agreement. The damping rate is harder to judge because the apparent amplitude consists of a complex superposition of interfering modes; nevertheless, the damping rate is low and appears to have roughly the same magnitude. Also recall that the precise character of the dipole modes will differ because of the difference in Hamiltonian.

Table 3: Peak central density contrast for $M(r_p) = 0.50$ and $m_p = 0.01$

W_0	r_p	r_{peak}	$\lvert\rho^s/\rho_0\rvert$	$M(r_{peak})$	t_{peak}
3	1.6	0.7	0.004	0.09	17.5
5	1.6	0.6	0.006	0.09	15.2
7	1.6	0.3	0.009	0.03	20.0

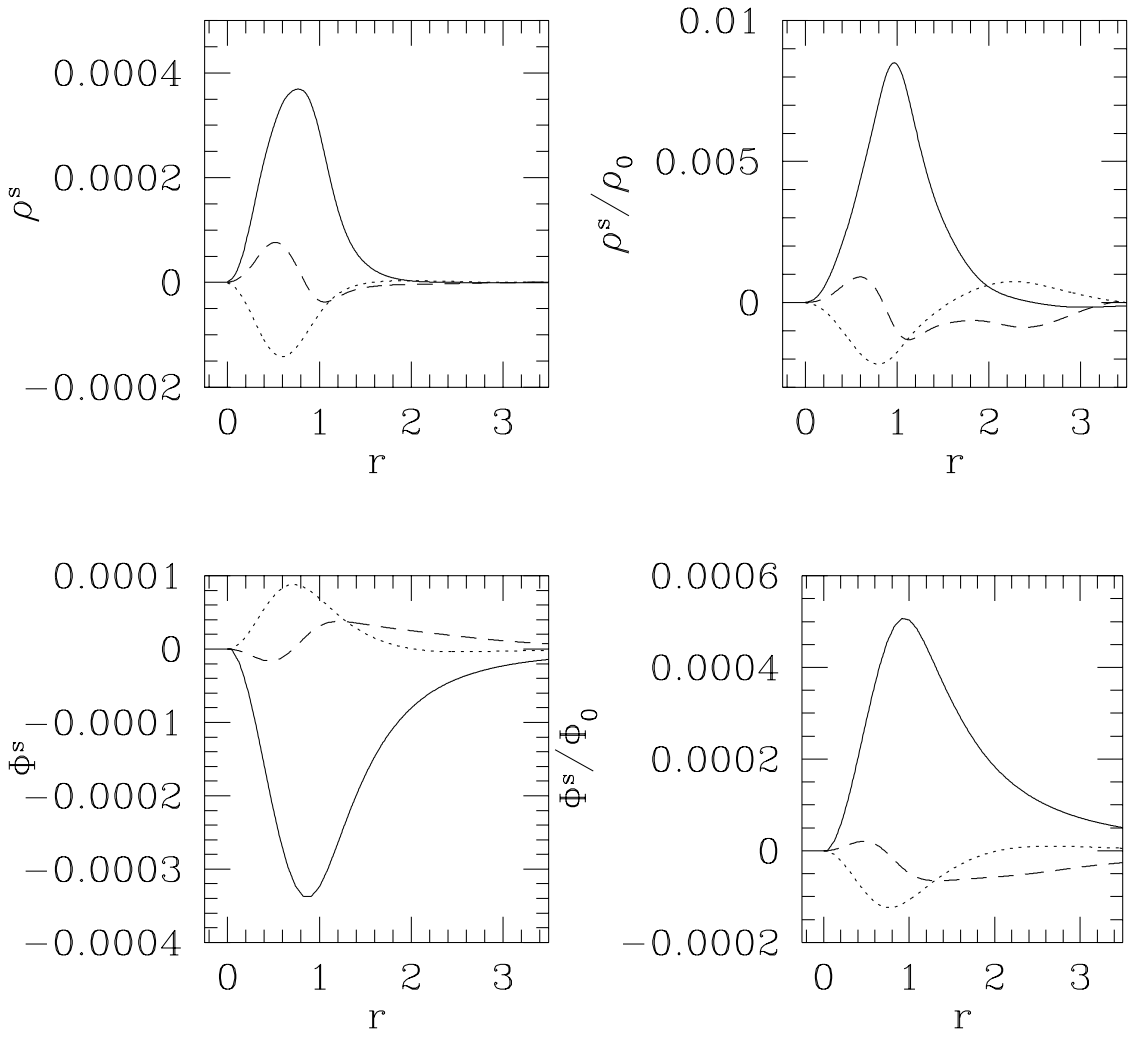

Fig. 6.— Transmission of quadrupole response in $W_0 = 5$ King model with $r_p = 1.0$ (25% mass radius) for $m_p = 0.01$. Panels are as in above figures with radial profile along $\mathbf{r}_p$. Solid line shows peak response at $t = 1.1$, immediately after perturbation. Dotted line and dashed lines show subsequent decay at $t = 3.4$ and $t = 5.7$, respectively.

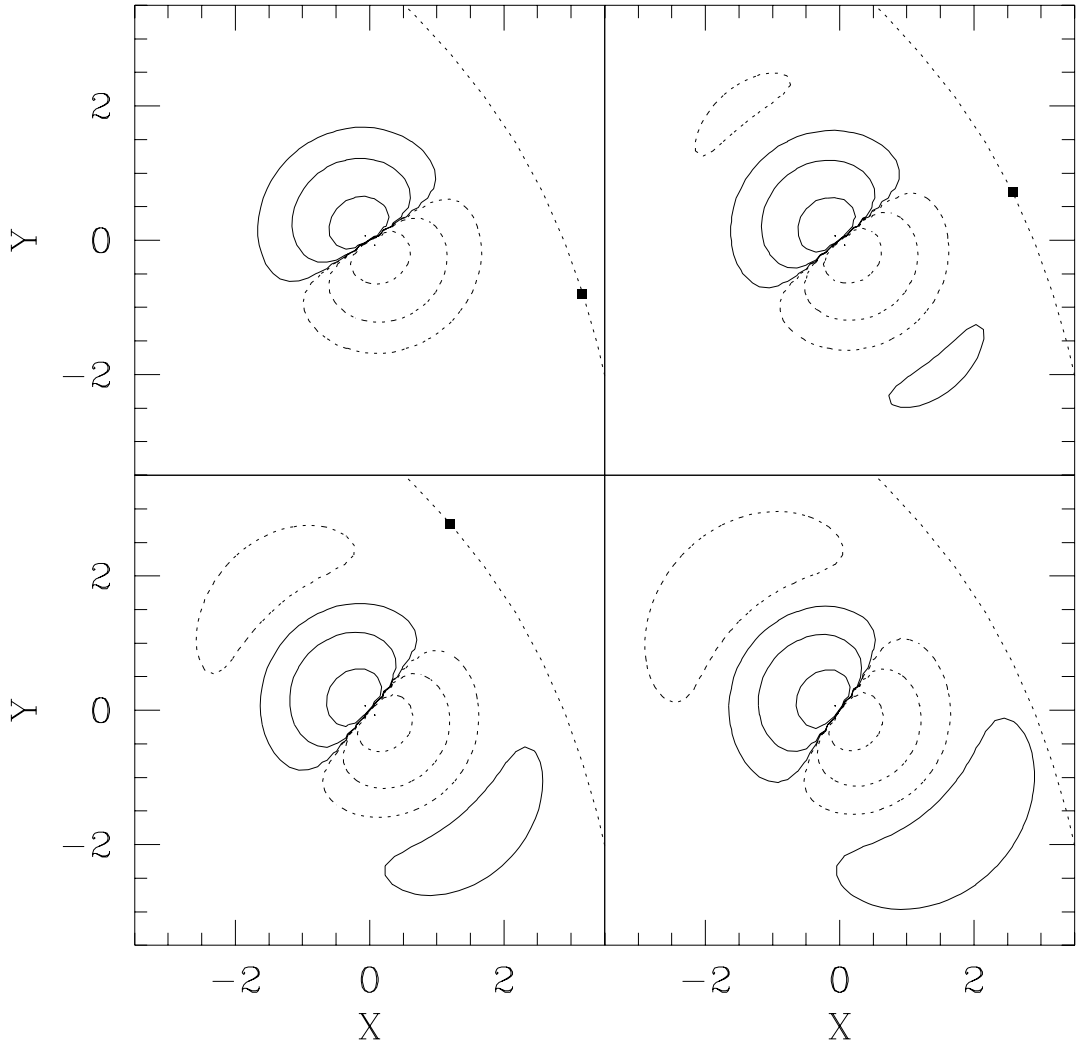

Fig. 7.— The dipole response induced by a point-mass perturber with $m_p = 0.01$ on a hyperbolic trajectory in the X-Y plane indicated by dotted curve in each panel. The solid square shows the perturber's position when in the field of view. Solid (dotted) contours show overdensity (underdensity) in unit logarithmic intervals, $\log \rho^s = -1, -2, -3$, about the peak at each time. Time interval $\Delta t = 2.44$ separates each panel. The peak density response is $\rho^s_{max} = 0.022, 0.032, 0.039, 0.042$ at $r_p = 0.2$ from left to right, top to bottom. The absolute maximum occurs in the final panel after the perturber has flown by and is roughly a 10% perturbation to the background density. The mode continues to librate through the center long after the perturber has passed.

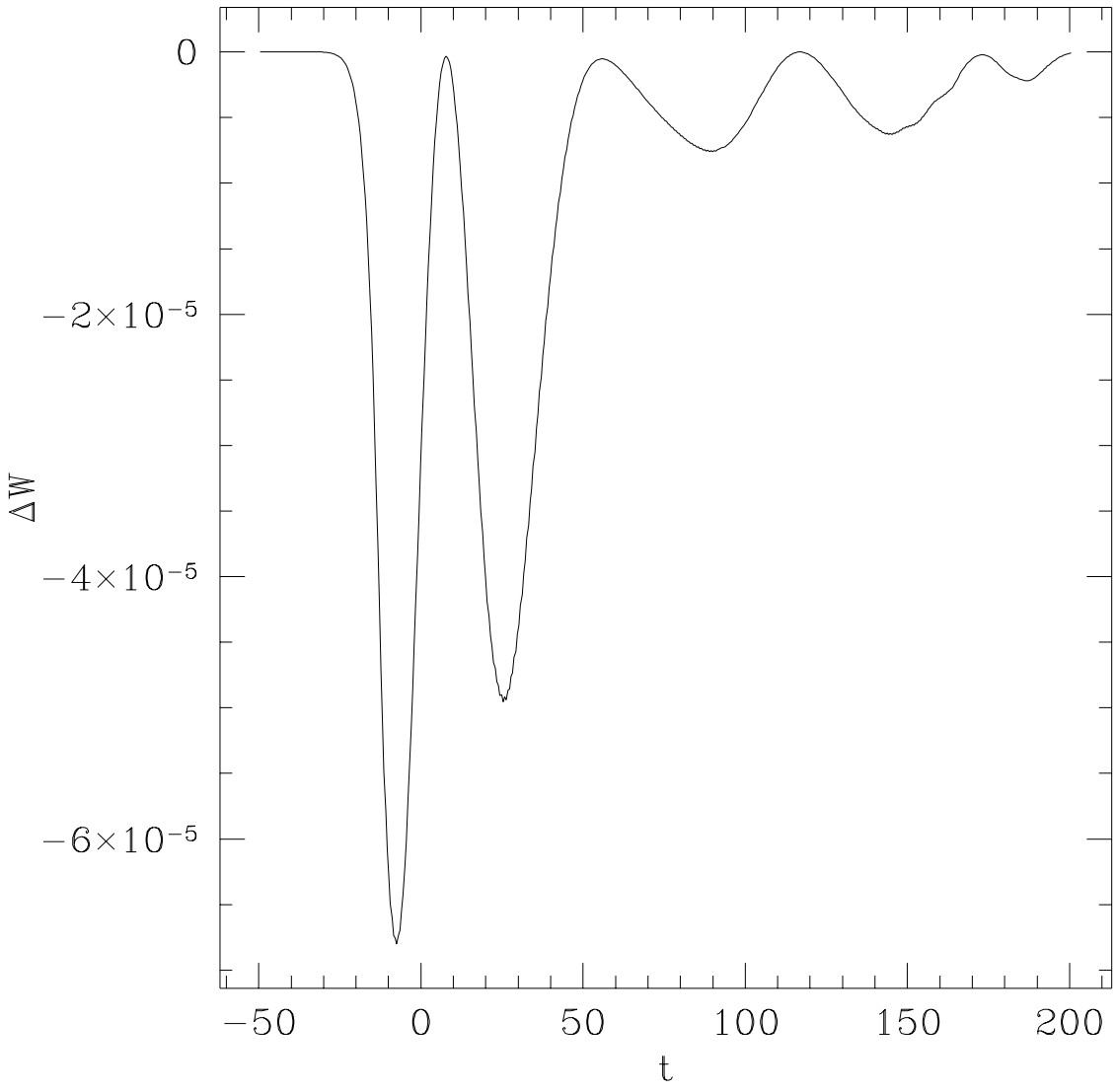

Fig. 8.— Potential energy perturbation as a function of time for $W_0 = 7$ system in Figure 5. The potential energy perturbation is only $\sim 3 \times 10^{-4}$ the potential energy of the entire system. The total initial disturbance decays rapidly but a fair amount of the input power persists in a weakly damped mode.

6. Discussion and Conclusions

Overall, our results indicate that halos can respond quite actively to perturbations. The response appears strong over a wide range of profiles and can efficiently transmit disturbances from the outer halo into the inner halo. In particular, the dipole response dominates and is strongest for the highest concentration system. The weak damping at high concentration may reflect kinematic decoupling of core and halo. The dipole response is still significant at low concentration but does not appear to persist in weakly damped modes. At low concentration, the monopole contribution can be fairly strong and long-range. The quadrupole response is roughly independent of concentration and seems to be more strongly excited through resonant forcing (Weinberg 1998).

Our results complement recent work by Weinberg (1994). The results appear to be consistent: mode shapes are similar; both calculations give roughly the same central displacement due to the dipole response; and the weakly damped dipole modes in the $W_0 = 7$ system appear to have nearly the same period and similar damping rates in both calculations. Furthermore, the present results suggest that it may be difficult to excite the weakly damped dipole modes in $W_0 = 3$ and $W_0 = 5$ King models discussed by Weinberg (1994).

More generally, the results suggest that noisy halos play a role in exciting disk structure and can drive evolution in the inner parts of galaxies. As an example, recent surveys of disk galaxies show a high frequency of lopsided galactic disks ($\sim 30\%$; Zaritsky & Rix 1997). The strong $\ell = 1$ response found in our calculations suggests that the halo has influence in these systems. In particular, a weakly damped $\ell = 1$ mode with a long period can induce an adiabatic $m = 1$ distortion in a disk. Scaling the $W_0 = 7$ results to a 200 kpc halo, we find that the location of peak response is roughly 4 kpc, which is consistent with typically observed distortion locations. Persistent modes are attractive also because, in many cases, there is no obvious companion to the galaxy in question. Thus a previous encounter can excite a long-lived mode that continues to slowly distort the disk long after the perturber has gone. Ultimately the disk response depends on the relative mass in the mode. This aspect will require further investigation.

Another significant possibility is that active halos strongly influence the formation of galactic disks. The standard scenario is that disks settle adiabatically into static dark halos (e.g. Dubinski 1994). However, the proto-galactic environment is likely to be extremely noisy, particularly in outer regions, so that the halo may perturb the disk by transmitting numerous disturbances into the inner galaxy. Moreover, the inner halo may continue to oscillate as it settles after initial collapse. Halo oscillations can easily perturb the disk through the time-dependent gravitational potential. Conversely, the structural integrity of observed disks set limits on the degree of disequilibrium in the proto-galactic halo.

The above calculations have proved extremely valuable because of their high precision: they provide further evidence that the very subtle influence of the halo plays a major role in determining the observed properties of disk galaxies. Nevertheless, we emphasize the need to improve and perhaps develop alternatives to the methods used herein. The main drawback of the above

method is the reliance on numerous expansions and the extreme care required in implementation. Moreover, we are limited to systems with spherical geometry whereas galaxies most likely come in a variety of shapes. However, commonly used N-body methods still seem far from achieving the sensitivity required to reproduce such subtle effects. To reproduce off-center modes might require direct N-body codes with at least 10^6 particles– still 1 to 2 orders of magnitude beyond current capabilities.

This research was supported by NSERC and the Fund for Astrophysical Research. I thank John Dubinski for discussion and for assistance in setting up the parallel field code. I also thank Phil Arras, Scott Tremaine, Ira Wasserman, Martin Weinberg, Dick Bond and Peter Goldreich for helpful discussion.

REFERENCES

Binney, J. J., & Tremaine, S. 1987, Galactic Dynamics (Princeton: Princeton University Press)

Dubinski, J. 1994, ApJ, 431, 617

Edmonds, A. R. 1960, Angular Momentum in Quantum Mechanics (Princeton: Princeton University Press).

Goldstein, H. 1980, Classical Mechanics, (Reading, MA: Addison-Wesley)

Hernquist, L. & Ostriker, J. P. 1992, ApJ 386, 375

Lynden-Bell, D. 1985, in The Milky Way Galaxy, eds. H. van Woerden et al. (Dordrecht: Reidel), 461

Kalnajs, A. J. 1977, ApJ, 212, 637

Murali, C. & Tremaine, S. 1998, MNRAS, 296, 749

Nelson, R. W., and Tremaine, S. 1996, "The dynamics of warped galaxies", in Gravitational Dynamics, O. Lahav, E. Terlevich and R. Terlevich, eds. (Cambridge: Cambridge University Press), 73

Nelson, R. W. & Tremaine, S. 1998, MNRAS, in press

Saha, P. 1991, MNRAS, 248,494

Tremaine, S. & Weinberg, M. D. 1984, MNRAS 209, 729

Tricomi, F. G. 1957, Integral Equations (New York: Interscience Publishers)

Weinberg, M. D. 1989, MNRAS 239, 549

Weinberg, M. D. 1991, ApJ, 368, 66

Weinberg, M. D. 1994, ApJ, 421, 481

Weinberg, M. D. 1995, 455, L31

Weinberg, M. D. 1998, MNRAS, 299, 499

Zaritsky, D. & Rix, H. W. 1997, ApJ, 477, 118

Zaritsky, D. & White, S. D. M. 1994, ApJ, 435, 599

This preprint was prepared with the AAS LaTeX macros v4.0.